



# Adsorbents from rice husk and shrimp shell for effective removal of heavy metals and reactive dyes in water<sup>☆</sup>

Md. Ibrahim H. Mondal<sup>a,1</sup>, Shovra Chandra Chakraborty<sup>a,1</sup>, Md Saifur Rahman<sup>b,1</sup>,  
Shaik Merkatour Hakim Marjuban<sup>c</sup>, Firoz Ahmed<sup>a,d</sup>, John L. Zhou<sup>e,\*</sup>,  
Mohammad Boshir Ahmed<sup>f,g</sup>, Masoumeh Zargar<sup>g</sup>

<sup>a</sup> Polymer and Textile Research Lab, Department of Applied Chemistry and Chemical Engineering, Rajshahi University, Rajshahi 6205, Bangladesh

<sup>b</sup> Department of Biomedical Engineering, Texas A&M University, College Station, TX 77843, USA

<sup>c</sup> Department of Materials Science and Engineering, Texas A&M University, College Station, TX 77843, USA

<sup>d</sup> BCSIR Laboratories Rajshahi, Bangladesh Council of Scientific and Industrial Research, Rajshahi 6206, Bangladesh

<sup>e</sup> Centre for Green Technology, School of Civil and Environmental Engineering, University of Technology Sydney, 15 Broadway, Sydney, NSW 2007, Australia

<sup>f</sup> Institute for Sustainability, Energy and Resources, School of Chemical Engineering, The University of Adelaide, North Terrace Campus, Adelaide 5005, Australia

<sup>g</sup> School of Engineering, Edith Cowan University, 6027 Joondalup, WA, Australia

## ARTICLE INFO

Handling Editor: Dr. Hocheol Song

### Keywords:

Chitosan  
Heavy metals  
Nano adsorbent  
Rice husk  
Solid waste

## ABSTRACT

Widespread contamination by heavy metals (HMs) and dyes poses a major health risk to people and ecosystems requiring effective treatment. In this work, rice husk (RH) and shrimp shells were extracted to obtain amorphous silica and chitosan, respectively, which were utilized to produce nano-chitosan-coated silica (NCCS). To ensure the stability of the nanoparticles, silica was freeze-dried after being coated with nano-chitosan. Functional groups ( $-NH_2$ ,  $-OH$ ,  $P/O$ ) from chitosan nanoparticles (CNPs) were introduced to the surface of silica during this process. Dyes such as brilliant green (BG), methylene blue (MB) and reactive brown (RB) as well as HMs ( $Cr^{6+}$ ,  $Pb^{2+}$ ,  $Cd^{2+}$ ,  $Ni^{2+}$ ) were removed by adsorbents. CNPs showed the highest adsorption capacity for RB (59.52 mg/g) among dyes and  $Cr^{6+}$  (42.55 mg/g) among HMs. CNPs showed the highest adsorption capacity for HMs among different adsorbents. Although NCCS and CNPs showed similar adsorption capabilities for HMs and dyes, NCCS showed the best stability. The adsorption performance decreased as  $RB > Cr^{6+} > MB > BG > Pb^{2+} > Cd^{2+} > Ni^{2+}$ . The adsorption reactions followed both pseudo-first-order and second-order kinetics, and was spontaneous from thermodynamic analysis. In summary, the waste-derived adsorbents demonstrated excellent potential for removing HMs and dyes from water, while supporting effective management solid waste.

## 1. Introduction

The demand for effective and sustainable solutions to address the rising pollution of heavy metals (HMs) and dyes in aquatic environments has prompted extensive research, in pursuit of a circular economy (Nnaji et al., 2023; Oulakhir et al., 2023). Bio-based materials, derived from living organisms, have gained significant attention due to their non-toxic nature and high abundance (Bădescu et al., 2018; Mojiri et al., 2022). Among these materials, rice husk (RH)-derived silica or silica nanoparticles stand out as promising nano-adsorbents for HMs and dye removal (Haider et al., 2022). The use of biogenic materials for

environmental applications has received widespread attention. RH as a major agricultural byproduct, demands proficient management Liu et al. (2013), Narayanasamy et al. (2022), Rendón et al. (2023).

While HMs such as Zn, Cu and Mn are essential trace elements for various organisms, others HMs ( $Pb^{2+}$ ,  $Cr^{6+}$ ,  $Cd^{2+}$ ,  $Hg^{2+}$ ) can cause harmful effects when present in high concentrations (Duffus, 2003). These toxic metals originate from natural sources and human activities (Nguyen et al., 2022), could bioaccumulate in food chains, posing health risks to different organisms (Zhou et al., 2001; Musilova et al., 2016). Consequently, the need for efficient removal of HMs becomes imperative, aligning with the broader goal of managing pollution and

<sup>☆</sup> This paper has been recommended for acceptance by Dr Hocheol Song.

\* Corresponding author.

E-mail address: [Junliang.Zhou@uts.edu.au](mailto:Junliang.Zhou@uts.edu.au) (J.L. Zhou).

<sup>1</sup> Equally contributed.

safeguarding ecosystems (Fu and Wang, 2011; Salman et al., 2019; Shamsollahi and Partovinia, 2019). Similarly, the adverse impacts of organic dyes on the environment have driven the search for effective strategies for their removal (Praveen et al., 2022). Synthetic and natural dyes are commonly used for various purposes including textiles and paper (Waghmare et al., 2023). Strict mitigation approaches are required due to the detrimental effects of certain dyes, especially reactive dyes, on water quality and ecosystems (Haider et al., 2022) and potential DNA damage in humans (Feng et al., 2012).

Silica nanoparticles have emerged as versatile candidates for HMs and dye removal (Yang et al., 2013; Shen et al., 2014), and are used in catalysis (Adam et al., 2012), biomedicine (Wang et al., 2012; Athinayanan et al., 2015) and biosensors (Yang et al., 2015). Despite their potential, there exist challenges including financial limitations and the requirement for in-depth research on nanoparticle interactions (He et al., 2015).

The abundant rice milling byproduct (i.e. RH) has garnered attention due to its high silica content (Liu et al., 2013; Haider et al., 2022). Its conversion into bio-oil, vapor, and biochar through thermochemical processes aligns with sustainable waste management practices (Bakar and Titiloye, 2013; Alvarez et al., 2014; Khonde and Chaurasia, 2016). RH ash (RHA) contains amorphous silica and offers diverse applications (Pode, 2016). The superior purity of silica resulting from acid treatment (HCl, H<sub>2</sub>SO<sub>4</sub>, HNO<sub>3</sub>) substantially enhances their adsorption capacity by eliminating metallic impurities (Yalcin and Sevinc, 2001; Bakar and Titiloye, 2013). Thermal treatment, on the other hand, produces low-purity silica despite its low cost (Rafatullah et al., 2010). Additionally, acid treatment promotes the protonation of the adsorbent surface, thus augmenting the positive surface charge density (Da'na, 2017). Numerous research on synthesizing silica nanoparticles from RH has resulted in high specific surface area (SSA) materials (Kumproa et al., 2012; Ang et al., 2013; Carmona et al., 2013).

Chitosan biopolymers with unique attributes such as biocompatibility, biodegradability and chelating properties, have shown effective performance in water purification (Dyal et al., 2003; Varma et al., 2004; Zhou et al., 2007). Chitosan is considered ideal for removing HMs and dyes due to its ability to form complexes and retain compounds (Jeon et al., 2001; Mourya and Inamdar, 2008). CNPs exhibit superior adsorption rates, which further enhances their efficacy in water treatment (Dyal et al., 2003; Olivera et al., 2016; Jain et al., 2021).

Silver, zinc and alumina nano-adsorbents have shown efficacy in removing toxic compounds from drinking water (Mauter and Elimelech, 2008). Activated carbon and carbon nanotubes are prominent choices due to their exceptional adsorption capabilities (Jain et al., 2021). In comparison, adsorbents made from microbes and agricultural waste could effectively remove pollutants while having biocompatibility and cost-effectiveness (Rafatullah et al., 2010; Oulakhir et al., 2023). Nano-adsorbent aerogels, having high porosity and large surface areas, are ideal for water purification. Natural polymer-derived aerogels gained attention due to biodegradability (Zhang et al., 2020). Therefore, natural biowastes have great potential to produce different adsorbents for environmental remediation applications (Mojiri et al., 2021). It is hypothesized that biowastes can be converted to valuable adsorbents with high adsorption capacity for HMs and organic dyes. Most research predominantly studies the removal of either heavy metals or organic dyes, with limited attention given to the simultaneous adsorption of both from complex wastewater. This scarcity of studies arises from the challenge posed by co-contaminated HMs and organic dyes, which compete for active sites on adsorbents and reduce adsorption capacity (Huang et al., 2022).

Hence, the objectives of this study were to extract silica and chitosan from RH and shrimp shells, to enhance the stability of nano-chitosan particles by developing a composite material with nano-chitosan-coated silica (NCCS), and to assess the adsorption capacity of these materials for HMs and dyes in water. Moreover, the study evaluated Langmuir and Freundlich adsorption isotherms to identify optimal

adsorption conditions.

## 2. Materials and methods

### 2.1. Materials

Sodium hydroxide (NaOH, MW 40 g/mol, purity  $\geq 97\%$ ), sodium carbonate (Na<sub>2</sub>CO<sub>3</sub>, purity  $>98\%$ ), acetic acid (CH<sub>3</sub>COOH), nickel chloride (NiCl<sub>2</sub>·6H<sub>2</sub>O, MW 237.69 g/mol, purity  $\geq 98\%$ ), and cadmium sulfate hydrate (CdSO<sub>4</sub>, MW 775.58 g/mol, purity  $\geq 99\%$ ) were purchased from Merck (India). Hydrochloric acid (37–38%), sulfuric acid (density 1.02 g/cm<sup>3</sup> at 20 °C), and potassium dichromate were purchased from Merck (Germany). Sodium lauryl sulfate (SLS, purity 99%) and Tween 80 surfactant (pH 6, density 1.08 g/cm<sup>3</sup>) were supplied by LOBA Chemie (India). Sodium tri-poly phosphate (STPP, MW 367.86 g/mol) was supplied by Sisco Research Laboratory (India). Lead acetate and brilliant green (BG) (MW 482.64 g/mol) were obtained from GURR and BDH laboratories. Reactive brown (RB) and methylene blue (MB) were purchased from Sigma Aldrich. Shrimp shell was collected from the Mongla Export Processing Zone, Bagerhat, Bangladesh. RH was collected from a rice mill in Katakhal, Rajshahi.

### 2.2. Extraction of amorphous silica from RH

RH was treated by sieving through a 40-mesh screen and treating with a sodium lauryl sulfate solution in a 1000 mL beaker for 30 min on a magnetic stirrer. After surfactant removal through air-oven drying at 110 °C for 6 h, the dried product was extracted for silica following a method by Haider et al. (2022). The washed sample underwent demineralization with a 1:15 mixture of 1N HCl and 1N H<sub>2</sub>SO<sub>4</sub> at 100 °C for 3 h with continuous stirring (500 rpm). The RH was then neutralized by rinsing with distilled water followed by filtration. Acid leaching of the RH using HCl and H<sub>2</sub>SO<sub>4</sub> was carried out and the resulting material was air-dried at 110 °C for 6 h. To obtain non-treated, HCl-treated, and H<sub>2</sub>SO<sub>4</sub>-treated silica, both un-leached and acid-leached RH was heated in a muffle furnace at 600 °C for 2 h to remove organic components (Fig. S1, Supplementary Information).

### 2.3. Extraction of chitosan from shrimp shell

The shrimp shells were first cleaned, dried, and crushed using a laboratory grinding mill with 60-mesh sieves. Shrimp shell powder was then mixed with 1N hydrochloric acid (1:20 W/V ratio) and heated at 105 °C for 4 h. The residue was filtered under a vacuum and washed with pure water. Afterward, the demineralized shrimp shells were dried at 65 °C for 4 h, then treated with 1N NaOH (1:15 ratio) to degrade proteins to form chitin. The chitin was neutralized with distilled water, followed by drying at 65 °C for 4 h. Refluxing was carried out using 150 mL of absolute acetone for 45 min followed by processing with 40% acetone. After two washes with distilled water, 0.3% NaOCl solution was used to treat the mixture, followed by distilled water washing and drying at 65 °C for 5 h. Deacetylation was achieved by mixing dried chitin with 40% NaOH solution (1:20) and heating at 100 °C for 3 h. Chitosan was purified through vacuum filtration with distilled water, then dried at 65 °C 4 h (Fig. S1).

### 2.4. Preparation of nano-chitosan

Ionic gelation process was used for nano-chitosan production. Chitosan powder (1.0 g) was dissolved in 1.0 L of 2.0% acetic acid solution, then the pH was adjusted to 4 by adding 0.5 N NaOH. To prevent nanoparticle aggregation, a 5% (v/v) Tween-80 surfactant solution was added. STPP concentration (1.0 mg/mL) was maintained by dissolving 0.5 g of STPP in 500 mL of distilled water. Both chitosan and STPP solutions were filtered using Whatman filter paper (Grade 42). Chitosan solution (100 mL) was mixed with STPP solution under magnetic stirring

at 800 rpm, then the suspension was centrifuged for 10 min at 8000 rpm. The collected nano-chitosan was re-suspended in deionized water, and then underwent another centrifugation process. CNP powder was obtained via freeze-drying the residual mass at  $-80\text{ }^{\circ}\text{C}$  (Fig. S1).

### 2.5. Preparation of NCCS

Untreated,  $\text{H}_2\text{SO}_4$ -treated, and HCl-treated silica were weighed and mixed for 10 h at 400 rpm, followed by immersion in a nano-chitosan suspension. They were filtered with grade 42 filter paper followed by freeze drying at  $-80\text{ }^{\circ}\text{C}$ . The product was labeled as non-treated NCCS,  $\text{H}_2\text{SO}_4$ -treated NCCS, and HCl-treated NCCS (Fig. S1).

### 2.6. Adsorption experiments

In adsorption experiments, solutions of MB, BG, RB,  $\text{Cr}^{6+}$ ,  $\text{Cd}^{2+}$ ,  $\text{Pb}^{2+}$  and  $\text{Ni}^{2+}$  (50 mg/L) were mixed with 30 mg of adsorbents (CNPs, silica, NCCS) for 0–50 min. After the treatment, the remaining concentration of the dyes was determined by a UV-Vis spectrophotometer, using maximum absorbance wavelength of 664.5 nm for MB, 502 nm for RB and 626 nm for BG. Atomic absorption spectroscopy (AAS) analysis was used for HMs analysis. The effect of pH on the adsorption of HMs and dyes was studied by adjusting solution pH to 2, 4, 6, 8 and 10 by 0.1 N HCl and NaOH. In addition, the effect of concentration of HMs or dyes was examined at pH 6.2. All experiments were carried out at least three times, and the average values were reported, together with standard error bars and correlation coefficient ( $R^2$  values) where applicable. For the determination of free energy change ( $\Delta G$ ) during adsorption, the Langmuir adsorption constant was used. Adsorption kinetics were studied and modeled by the pseudo-first-order and second-order

reaction kinetics.

### 2.7. Characterization

The concentrations of HMs and dyes in adsorption experiments were determined by AAS (Model AA-6880, Shimadzu, Japan) and a UV-visible Spectrophotometer (Model UV-1900i, Shimadzu, Japan), respectively. Attenuated total reflection-Fourier transform infrared (ATR-FTIR) spectroscopy was used for the identification of functional groups in adsorbents. Adsorbents were also examined by a field emission scanning electron microscope (FESEM) (Model JSM-7610F, JOEL Ltd, Tokyo, Japan) to determine their surface properties, and by X-ray diffractometer (XRD) (Model Rigaku, SmartLab) to determine their crystallinity. Thermogravimetric analysis (TGA) (Model STA 8000, PerkinElmer, Netherlands) was used to understand the sample weight loss with respect to temperature changes. Differential thermal analysis (DTA) (Model STA 8000, PerkinElmer, Netherlands) was also performed.

## 3. Results and discussion

### 3.1. Surface morphology and surface area of adsorbents

Silica and NCCS were subjected to SEM analysis to determine the morphology (Fig. S2), indicating the presence of nanoparticles ( $<100\text{ nm}$ ). The morphology of NCCS particles appeared larger compared to silica, indicating the attachment of CNPs on silica surface due to the formation of a composite structure. Between silica and CNPs, weak interactions such as van der Waals interactions and hydrogen bonds were expected to dominate as the preparation process did not involve post-

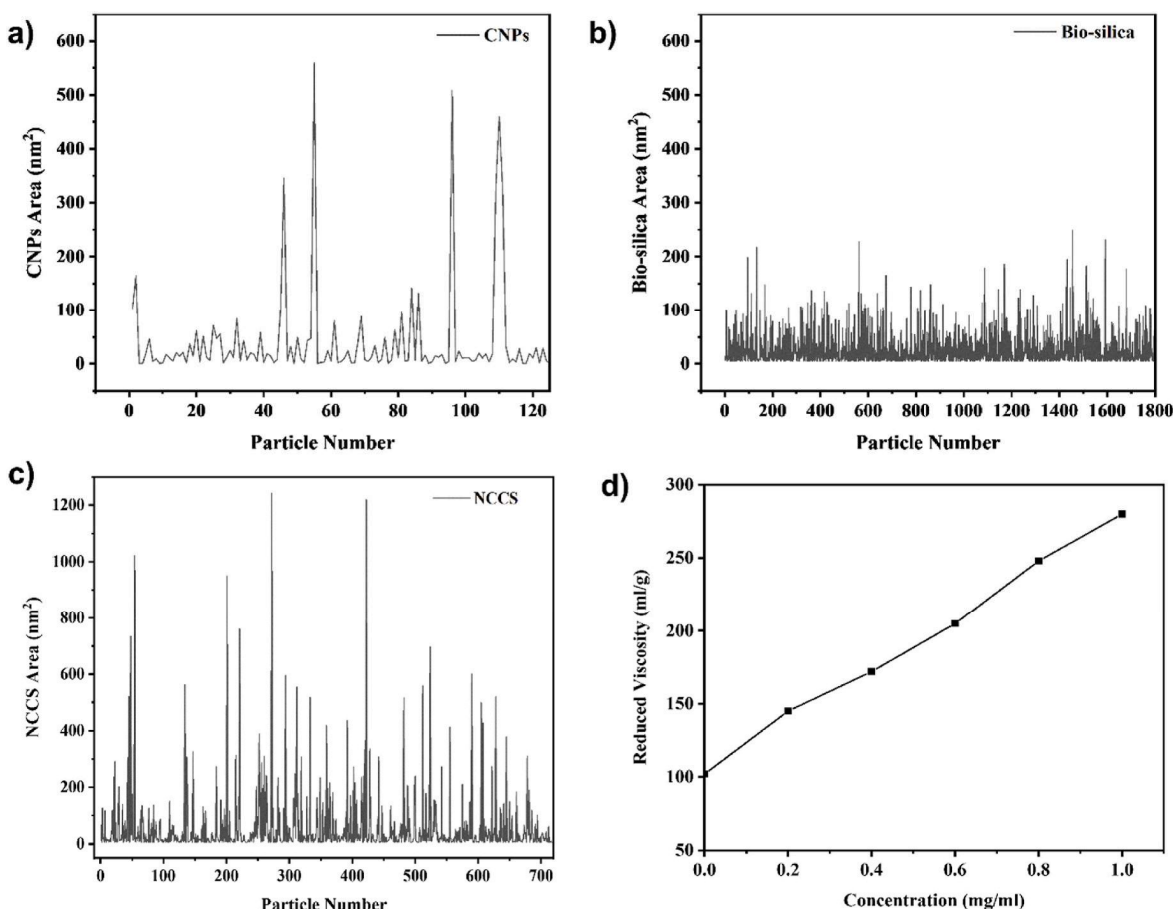


Fig. 1. Particle size distribution of (a) CNPs, (b) bio-silica, (c) NCCS, and (d) reduced viscosity vs. concentration graph of chitosan solution.

annealing except only freeze-drying. Therefore, NCCS showed better compositional stability.

The size and SSA of nanoparticles in SEM images were determined using ImageJ software (Fig. 1). Fig. 1a–c shows the particle size distribution curves for CNPs, silica, and NCCS, which followed the order of silica < CNPs < NCCS. The particle size of NCCS was large due to the CNPs coating on nano-silica surface. All particle sizes in the nano range were confirmed by FESEM analysis. The molecular weight of chitosan was determined using the viscometrical method (Fig. 1d). The viscosity average molecular weight of chitosan (10 mg/mL, 0.8 mg/mL, 0.6 mg/mL, 0.4 mg/mL, 0.2 mg/mL) was analyzed after being dissolved in acetic acid and NaCl solution. The reduced viscosity was determined by analyzing the solution using Ostwald's viscometer. The reduced viscosity increased with the increase in chitosan solution concentration (Fig. 1d). The viscosity average molecular weight of chitosan was estimated to be 82803.620 Da based on the Mark-Houwink equation.

SSA of CNPs, silica, and NCCS can be calculated by the MB dye adsorption method considering the monolayer MB adsorption (Eq. (1)).

$$SSA = X_m \times N \times A \quad (1)$$

where  $X_m$  is the monolayer adsorption capacity which can be derived from the Langmuir adsorption isotherm,  $N$  is Avogadro's number ( $6.023 \times 10^{23}$ ) and  $A$  is the area adsorbed by per molecule of methylene blue ( $130 \text{ \AA}^2$ ). The highest monolayer adsorption capacity values were found for  $\text{H}_2\text{SO}_4$ -treated NCCS (47.6 mol/g) and CNPs (48.3 mol/g) compared to non-treated silica as well as HCl-treated silica (Table S1). This primarily indicates the adsorption behavior of the extracted and prepared materials. This data was also correlated with the specific adsorption surface areas of the materials. Similar to monolayer adsorption capacity values,  $\text{H}_2\text{SO}_4$ -treated NCCS, and CNPs also showed a higher SSA than other prepared silica. It appears that the adsorption behavior of sulfuric acid-treated NCCS and CNPs would follow a similar pattern since their monolayer adsorption capacity was comparable. However, compared to silica particles and CNPs, the coated structure has better stability to deal with continuous contaminant removal.

### 3.2. Thermal analysis of RH, CNPs and NCCS

To understand the thermal stability, thermal degradation, and reaction properties of RH, CNPs, and NCCS, TGA and DTA were conducted from 30 to 800 °C by a simultaneous thermal analyzer machine (STA 8000, PekinElmer, Netherland). The thermal stability sequence decreased as NCCS > CNPs > RH. For RH samples, the thermal weight loss can be described in three stages (Fig. S3a). The initial weight loss of RH (~5%) occurred at a temperature of 30–250 °C due to the loss of water and other volatile substances. In the second stage (280–360 °C), a rapid and maximum weight loss (50–60%) occurred due to the thermal decomposition of hemicellulose and cellulose in RH (Lü et al., 2017). In the third stage, 20–25% weight loss occurred from lignin. Lignin is a thermally stable aromatic polymer (Das et al., 2013), which decomposes at 370–600 °C. The residual ash mainly consisted of non-combustible silica (~15%, >600 °C).

Of prepared RH, acid-leached RH showed lower thermal stability than un-leached RH due to acid hydrolysis. Because of acid treatment, cellulose and hemicellulose broke into lower molecular weight compounds, which were thermo-degraded easily. For CNPs, ~7% weight loss first occurred at ~100 °C due to the evaporation of bound and unbound water. The maximum weight loss occurred at 230–280 °C, which corresponded to a complex process including the dehydration of saccharide rings, depolymerization, and decomposition of acetylated and deacetylated units of polymer (Das et al., 2013). The NCCS showed the highest thermal stability and a low residual weight loss as the extracted silica was used in the composite preparation. Two thermal stages of weight loss (30–230 °C, 230–550 °C) occurred during the heating of NCCS (Fu and Wang, 2011). In stage 1, ~5% of the weight

was lost due to moisture. Stage 2 was related to the decomposition of nano-chitosan which completely burned at 550 °C. The amount of coated CNPs on silica surface was determined to be ~10%, which was equivalent to the increased weight of silica after coating with nano-chitosan.

The exothermic and endothermic behavior of adsorbents under temperatures 30–800 °C was identified by DTA analysis. For all samples, a common endothermic reaction occurred near 65 °C attributed to water release from samples (Fig. S3b). Considering RH samples, both  $\text{H}_2\text{SO}_4$ -treated and HCl-treated RH had the same exothermic peaks at 360 °C and 530 °C, and endothermic peaks at 460 °C and 610 °C. RH demonstrated exothermic peaks at 360 °C and 487 °C, and endothermic peaks at 400 °C and 535 °C. The CNPs and NCCS showed exothermic peaks at 500 °C and 530 °C, respectively.

### 3.3. Crystallinity and surface functional groups of adsorbents

To investigate the role of acid in modifying silica, structural analyses of dry-annealed films were conducted using XRD. The acid-leached silica showed completely amorphous structures upon combustion below 700 °C because of the removal of alkali metals (Khonde and Chaurasia, 2016). Acid treatment of RH did not affect the silica structure. The broad peak with maximum intensity at  $2\theta = 21.57^\circ$  was observed, indicating the amorphous nature of silica (Fig. 2a).

The FTIR spectra of pristine silica and acid-modified silica (HCl and  $\text{H}_2\text{SO}_4$ ) are presented in Fig. 2b, with no significant difference before and after acid treatment. The IR peaks at  $447 \text{ cm}^{-1}$ ,  $799 \text{ cm}^{-1}$  and  $1063 \text{ cm}^{-1}$  indicated Si–O–Si bond rocking, bending, and stretching vibrations, respectively (Liu et al., 2006). As shown in Table S2 and Fig. 2c, nano chitosan showed different bands than pristine chitosan. Chitosan exhibited a peak at  $3439 \text{ cm}^{-1}$  representing the  $-\text{NH}_2$  functional group, which shifted to  $3260 \text{ cm}^{-1}$  in nano chitosan, indicating the crosslinking between sodium tripolyphosphate and chitosan. The peaks at  $1640 \text{ cm}^{-1}$  and  $1585 \text{ cm}^{-1}$  can be attributed to  $-\text{CONH}_2$  and  $-\text{NH}_2$  groups, respectively, which shifted hypsochromically to  $1620 \text{ cm}^{-1}$  and  $1535 \text{ cm}^{-1}$  in nano-chitosan due to the interaction between  $-\text{NH}_3^+$  groups of chitosan and phosphate groups of TPP. This interaction was also supported by the decrease in amide band I ( $1640 \text{ cm}^{-1}$ ) intensity in CNPs compared to chitosan, indicating that amide and  $-\text{NH}_2$  groups in chitosan were crosslinked with TPP. The presence of a new peak at  $1220 \text{ cm}^{-1}$  (PJO stretching) proved the formation of nanoparticles from chitosan by the ionotropic gelation method.

The FTIR spectra (Fig. 2d) show silica and CNP functional groups of acid-modified samples. The peaks at  $452 \text{ cm}^{-1}$ ,  $793 \text{ cm}^{-1}$  and  $1068 \text{ cm}^{-1}$  were related to silica's Si–O–Si bending and stretching. The peaks at  $3258 \text{ cm}^{-1}$  and  $1555 \text{ cm}^{-1}$  indicated the stretching of  $-\text{OH}$  and  $-\text{NH}_2$  functional groups, respectively. The peaks at  $1622 \text{ cm}^{-1}$ ,  $1377 \text{ cm}^{-1}$  and  $1310 \text{ cm}^{-1}$  from the amide group and  $1030 \text{ cm}^{-1}$  from the PJO group were present in CNPs, confirming the attachment of CNPs on silica surface.

Based on FTIR spectra, it is inferred that mainly van der Waals interactions and hydrogen bond formation occurred between silica and CNPs. More specifically, silica has a Si–O–Si bond, whereas CNPs have  $-\text{NH}_2$ ,  $-\text{OH}$ , and  $-\text{O}-$  functional groups on their surfaces. Weak interactions such as hydrogen bond and van der Waals forces were expected to occur between silica-based oxygen and metallic silica groups and chitosan-based amine and hydroxyl groups. In addition, amine groups might partially contribute to the enhanced stability of NCCS. However, strong interactions were ruled out as no post-chemical or annealing process was used except freeze drying. In addition, the structure of NCCS was confirmed from FTIR and SEM analysis, showing larger NCCS particles than silica and effective attachment of CNPs on silica surface. Therefore, the stability of NCCS was greater than CNPs or nano silica alone.

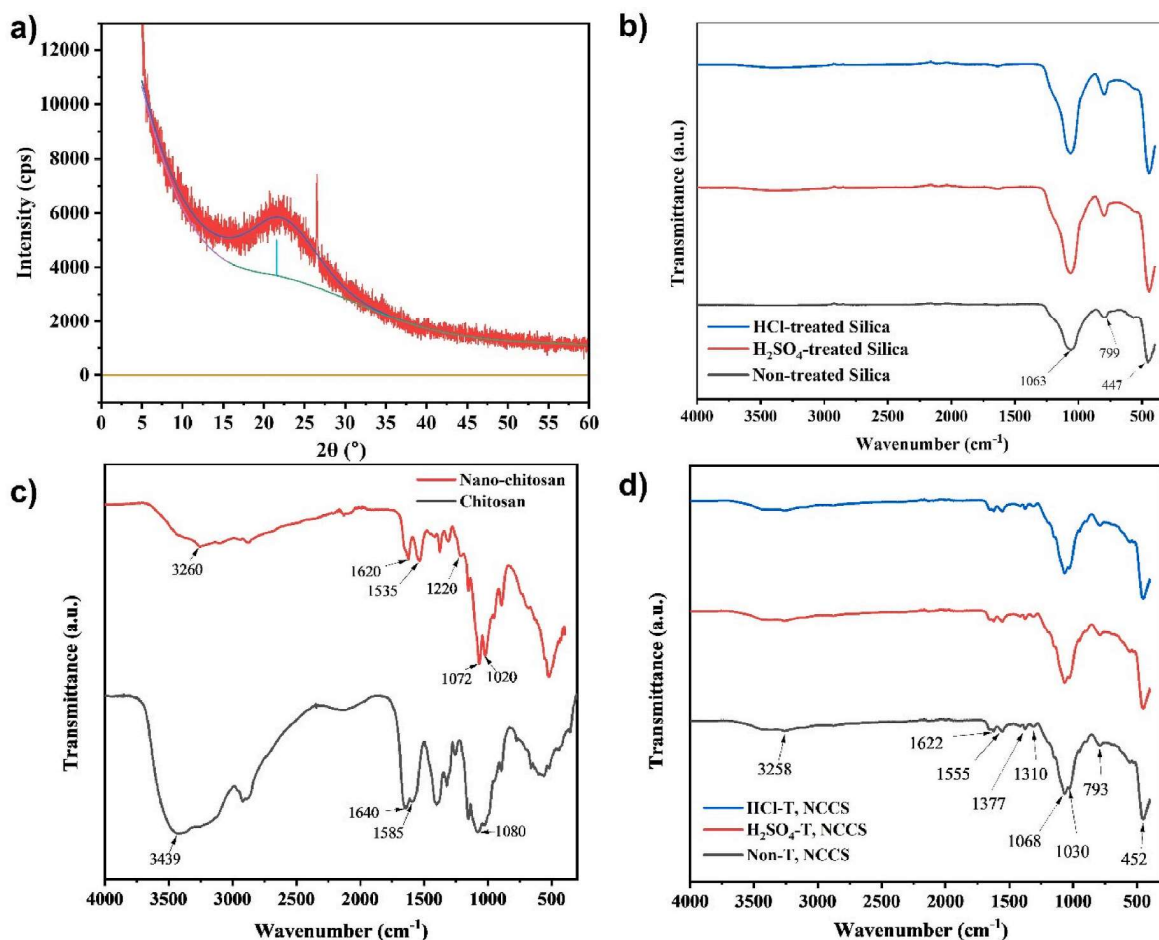


Fig. 2. (a) XRD of  $\text{H}_2\text{SO}_4$ -treated silica. FTIR spectra of (b) silica, (c) chitosan and (d) nano-chitosan NCCS.

### 3.4. Adsorption by CNPs, silica and NCCS

#### 3.4.1. Effect of contact time on pollutant adsorption

For CNPs, the adsorption capacity increased with contact time, and maximum adsorption capacity was obtained at 50 min, suggesting a time-dependent process. CNPs showed maximum adsorption capacity for RB dye among all dyes and  $\text{Cr}^{6+}$  among HMs. The main reason for this high adsorption capacity was due to the anionic nature of RB that can easily bind to  $-\text{NH}_2$  groups of CNPs (Fig. 3a). Therefore, electrostatic interactions are expected between adsorbent surface and adsorbate molecule.

For biosilica, the adsorption capacity also increased with contact time, achieving the maximum adsorption capacity at 50 min. Biosilica showed maximum adsorption capacity for MB among dyes and  $\text{Cr}^{6+}$  among HMs. CNPs showed a higher adsorption affinity toward RB. However, the adsorption capacity of HMs and dyes on silica was lower than CNPs because  $-\text{NH}_2$  and  $-\text{OH}$  groups were absent with only silanol group ( $\text{Si}-\text{O}^-$ ) being present for adsorption (Fig. 3b). In addition, silica had a lower SSA than CNPs. Eventually, all these factors contributed to lower adsorption capacities of silica particles than CNPs.

For NCCS, the adsorption capacity increased with time, and showed maximum adsorption capacity for MB among dyes and  $\text{Cr}^{6+}$  among HMs. The adsorption capacity of NCCS was higher than nano-silica, which could be due to the presence of silanol group ( $\text{Si}-\text{O}^-$ ) of silica and  $-\text{NH}_2$  and  $-\text{OH}$  group of CNPs (Fig. 3c). Therefore, NCCS showed higher adsorption capacities than nano-silica, but slightly lower than CNPs. This can be explained by the fact that in NCCS both silica and CNPs combined and blocked some pores in CNPs. However, the stability of NCCS was much better than nano-silica or CNP.

#### 3.4.2. Effect of pH on adsorption capacity

Solution pH could affect contaminant solubility, and ionization and functional group on adsorbent. The adsorption capacity of CNPs was found to be higher in acidic pH for RB and  $\text{Cr}^{6+}$ , and in the neutral pH range for other dyes (Fig. 3d–f). The adsorption capacity was low for all dyes and HMs under basic condition, due to the lower availability of surface charge of the adsorbents. The cationic functional groups ( $-\text{NH}_3^+$ ,  $\text{Si}^{4+}$ ) for silica and CNPs adsorbents are more than anionic sites at low pH, which can chelate dye and HM ions by electrostatic attractions (Fig. S4). At lower pH, similar range of adsorption capacity for  $\text{Cd}^{2+}$  can be observed using chitosan and its derivatives (Borsagli and Borsagli, 2019). In the alkaline condition, more  $\text{OH}^-$  ions impede anionic dye adsorption due to repulsion forces. RB is an anionic dye and binds to cationic sites at low pH. At low pH, CNPs adsorbed higher amounts of  $\text{Cr}^{6+}$ . Under basic conditions, all metal ions became precipitated as the hydroxides with negligible adsorption capacity (Fig. 3d, Fig. S4), as also reported by Zeng et al. (2015). The adsorption capacity of bio-silica for cationic dyes (BG and MB) was high (49 mg/g) under basic conditions while being low for anionic RB dye. For HMs,  $\text{Cr}^{6+}$  showed a higher adsorption capacity in acidic condition while other HMs showed higher adsorption capacity in the neutral pH range, due to pH effect on the binding sites on adsorbents. Hydrogen ions may compete strongly at low pH with HM ions. Silica mainly adsorbed HMs and dyes by the formation of dye-silica complex and metal-silica complex. However, the overall adsorption capacity of silica was lower than CNPs because of less binding sites (Fig. 3e, Fig. S4). For example, the adsorption capacity of CNPs for  $\text{Pb}^{2+}$  at pH 6 reached its peak (17 mg/g), a value comparable to the adsorption capacity of 19.55 mg/g observed for magnetic  $\text{Fe}_3\text{O}_4@$ -chitosan nanoparticles (Huang et al., 2022).

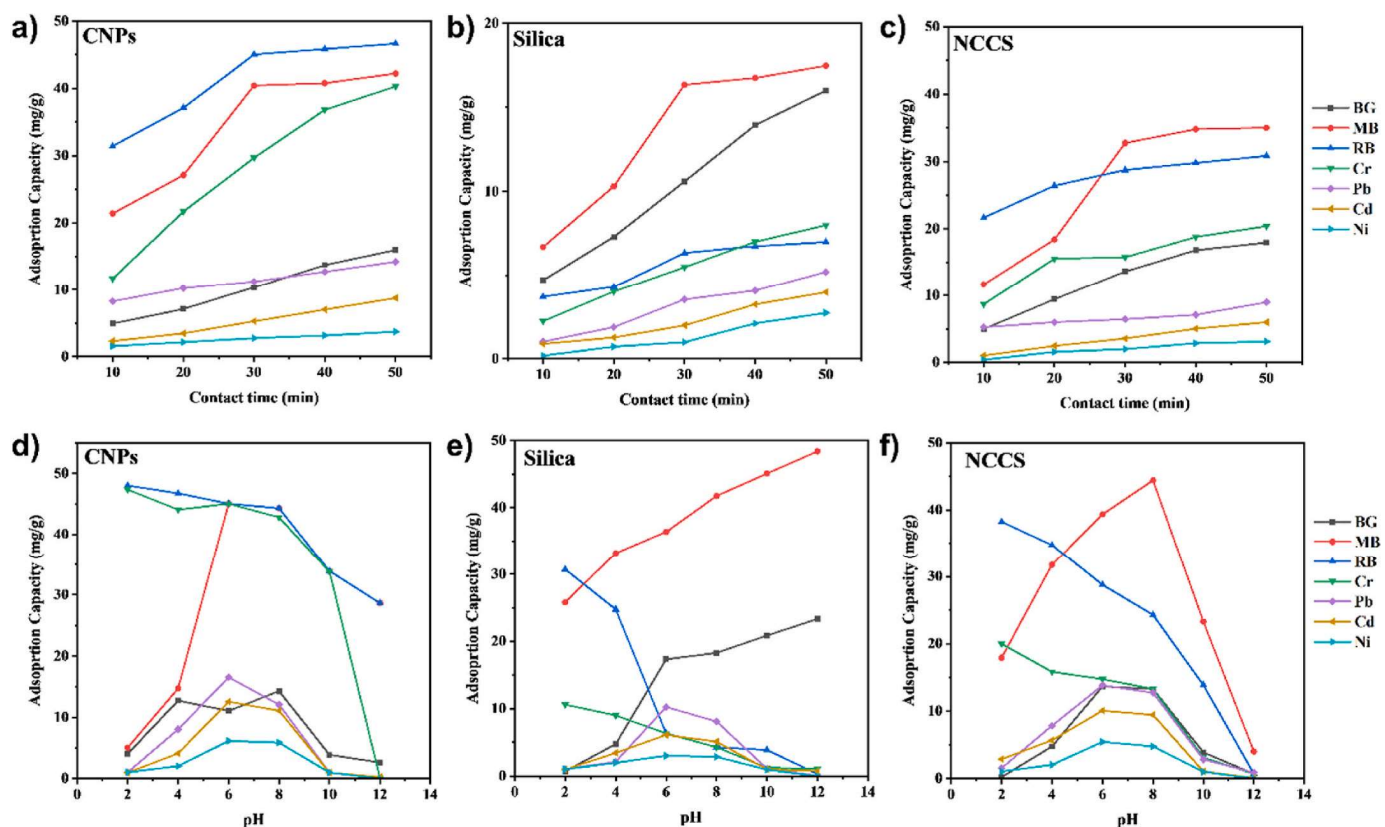


**Fig. 3.** Effect of contact time on HMs and dye adsorption for (a) CNPs, (b) silica, and (c) NCCS. Effect of pH on HMs and dye adsorption for (d) CNPs, (e) silica, and (f) NCCS.

A slightly acidic medium was favorable for maximum sorption of dyes and HMs. The  $pK_a$  value of adsorbents with  $-OH$  groups is above 8, hence at lower pH, mainly  $-O-$  groups and  $-NH_2$  groups from CNPs contributed to the adsorption processes. The adsorption capacity of NCCS showed the same adsorption property as CNP where the adsorption of RB (38 mg/g) and  $Cr^{6+}$  (20 mg/g) was higher under acidic conditions. At very low pH, NCCS is negatively charged, and can accumulate a higher amount of cationic dye RB. However, this effect becomes weaker with increasing pH, while the chelating power of NCCS became stronger with increasing pH in the acidic region, while RB and  $Cr^{6+}$  remain in a highly ionic state. In the alkaline pH, due to repulsion forces, more OH-ions impede anionic dye adsorption. RB is an anionic dye, and binds more significantly with more cationic sites at low pH. At basic pH, all metal ions became precipitated as hydroxides and showed negligible adsorption capacity (Fig. S4). The adsorption capacity of NCCS is more than CNPs and silica, as NCCS has the combined property of both silica and CNPs (Fig. 3f). For HMs and dyes, pH 6.2 resulted in a higher adsorption. The increased adsorption capacity around pH 6 was also reported for  $Pb^{2+}$  by amidated adsorbents (Huang et al., 2022).

### 3.4.3. Adsorption kinetics of CNPs, silica and NCCS

Pseudo-first-order reaction kinetics and second-order reaction kinetics were used to determine the adsorption reaction kinetics parameters, by plotting  $\ln(q_e - q_t)$  versus time ( $t$ ) and  $t/q_t$  against  $t$ , respectively. The kinetics parameters of CNPs, silica and NCCS are summarized in Fig. 4 and Tables S3–S5.

Considering the adsorption capacities, NCCS was found to be more active than silica, but lower than CNPs for HMs and dyes. The values of PFO and PSO rate constants ( $k_1$  and  $k_2$ ) were also found to be identical. The kinetics rate constant values for HMs adsorption by NCCS were lower than by CNPs but higher than silica. PSO-based equilibrium adsorption values of BG, MB, RB,  $Cr^{6+}$ ,  $Pb^{2+}$ ,  $Cd^{2+}$  and  $Ni^{2+}$  were higher

than PFO equilibrium values. The CNPs performed well except for MB. Higher equilibrium adsorption capacities were found for CNPs compared to NCCS, which could be due to the nature of composite formation. As silica has low adsorption capacities, the composite materials tend to sacrifice certain functional groups during surface coating of silica with CNPs. In addition, the  $R^2$  values of PFO and PSO were significant for all adsorbents (Table S3). The results tend to indicate that both physisorption and chemisorption processes were occurring during the removal of HMs and dyes.

### 3.4.4. Adsorption isotherms

The Langmuir isotherm (Eq. (2)) indicated the formation of a monolayer adsorbate on the surface of the adsorbent containing a finite number of identical sites (Dada et al., 2012):

$$\frac{1}{q_e} = \frac{1}{q_m} + \frac{1}{q_m K_L} \times \frac{1}{C_e} \quad (2)$$

where  $q_m$  (mg/g) and  $K_L$  (L/mg) are the Langmuir constants related to the maximum monolayer adsorption capacity and energy of adsorption respectively.  $q_e$  is the equilibrium adsorption capacity (mg/g), and  $C_e$  is the equilibrium concentration of dye/HM in solution (mg/L). In addition, the separation factor ( $R_L$ ) can be calculated, which can be classified as:

- i. For unfavorable adsorption if  $R_L > 1$ ,
- ii. For linear adsorption  $R_L = 1$ ,
- iii. For favorable adsorption  $R_L < 1$ ,
- iv. For irreversible adsorption  $R_L = 0$ .

In comparison, the Freundlich isotherm described the heterogenous surface adsorption process, as shown in Eq. (3):

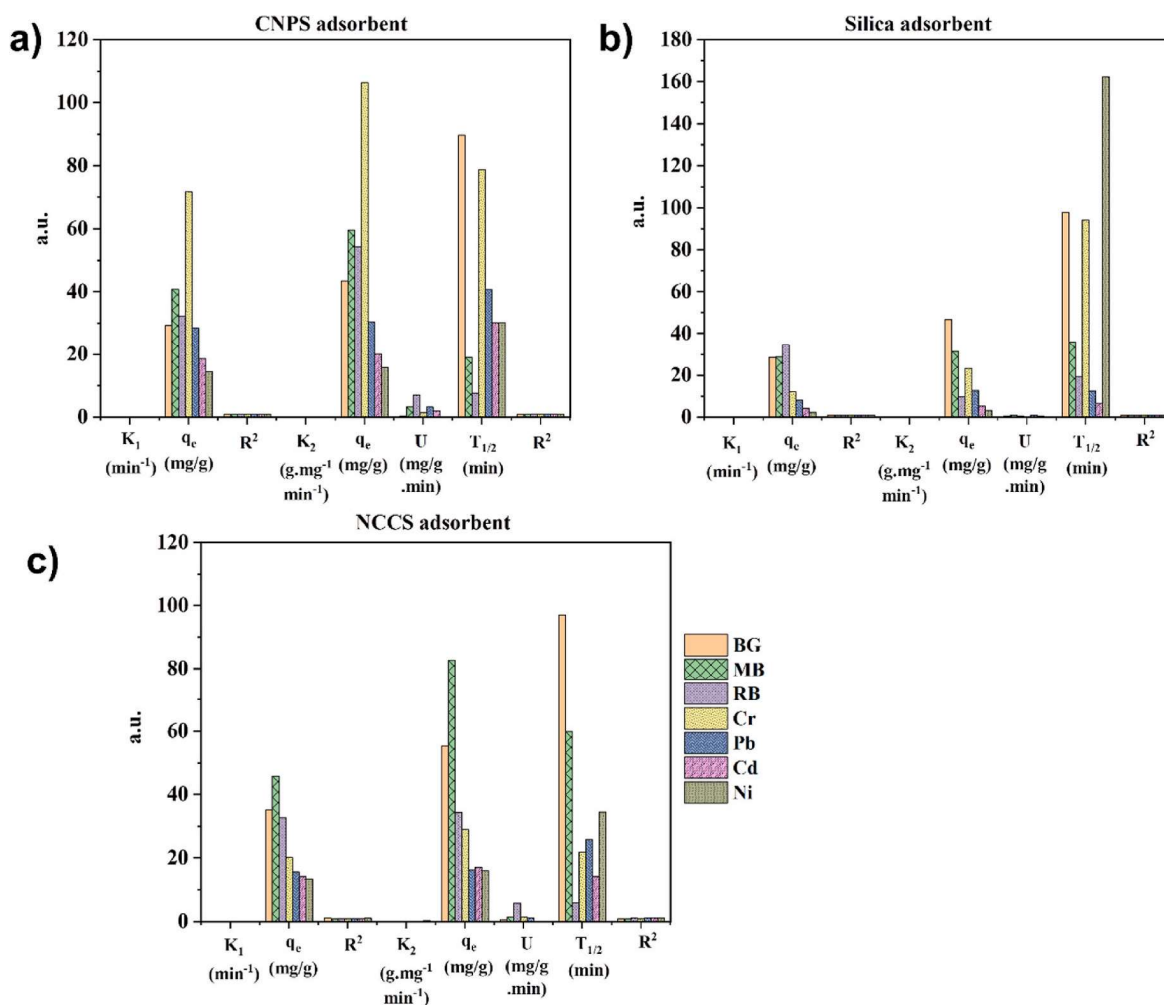


Fig. 4. Adsorption kinetics for (a) CNPs, (b) silica, and (c) NCCS adsorbents.

$$\log q_e = \log K_f + \frac{1}{n} \log C_e \quad (3)$$

where  $K_f$  is the Freundlich constant ( $\text{mg}^{(1-1/n)} \text{L}^{1/n}/\text{g}$ ) related to the bonding energy and  $1/n$  is a measure of deviation from linearity of adsorption.

The adsorption process can be independent of adsorbate concentration if  $1/n = 1$ , or a favorable adsorption if  $1/n$  value is  $< 1$ , or cooperative adsorption if  $1/n$  is  $> 1$  (Fu and Wang, 2011). A plot of  $\log q_e$  against  $\log C_e$  resulted in a straight line, where the values of  $n$  and  $K_f$  can be obtained from the slope and the intercept.

The  $R_L$  values for HMs and dyes were found to be very low for CNP and NCCS compared to biosilica, indicating that adsorption was mostly favorable for CNP and NCCS in comparison to biosilica (Tables S6 and S7). Based on Table S6 and Fig. 5, the value of  $n$  was higher than one except in a few cases indicating favorable adsorption. The  $R^2$  value of Langmuir adsorption was also higher than Freundlich isotherm for all adsorbents, indicating that adsorption was more towards monolayer coverage. Overall, the results suggest that the adsorption process involved both monolayer and multilayer adsorption. In all cases, the adsorption capacity values for CNPs and NCCS were found to be higher than that of acid-treated bio-silica.

In addition to porosity, nanosilica has a lone silanol group which can bind metal ions or dyes in an acidic environment through silicon metal-assisted interactions such as weak electrostatic interactions (Fig. S4). However, silica has less abundant freely accessible functional groups, than CNPs with abundant surface functional groups ( $-\text{NH}_2$ ,  $-\text{OH}$ ) which

can interact with metals or dyes to form electrostatic and weak hydrogen bonds (Fig. S4). Thereby, CNPs adsorption capacity was increased. On the other hand, some functional groups in NCCS participated in forming a stable composite, therefore might not be available for interaction with the contaminants. Therefore, CNP and NCCS demonstrated high adsorption capacities for most HMs and dyes. Overall, NCCS and CNP had shown similar performance in the adsorption process, although the stability of NCCS was higher than CNPs.

#### 3.4.5. Adsorption thermodynamics

In thermodynamics, the change in free energy can be determined by using Langmuir constant  $K_L$  as shown in Eq. (4):

$$\Delta G = - RT \ln K_L \quad (4)$$

where  $R$  is the molar gas constant ( $8.314 \text{ J}/(\text{K mol})$ ) and  $T$  is the absolute temperature. Table S7 shows thermodynamic parameters for the adsorption of dyes and HMs onto CNPs, silica, and NCCS. The free energy change is negative for all adsorption processes, indicating spontaneous and thermodynamically favorable adsorption of dyes and HMs on adsorbents.

## 4. Conclusions

Three novel adsorbents (silica, CNP, NCCS) were prepared from solid waste rice husks and shrimp shells for removing HMs and dyes from water, following synthesis and characterization. The highest adsorption

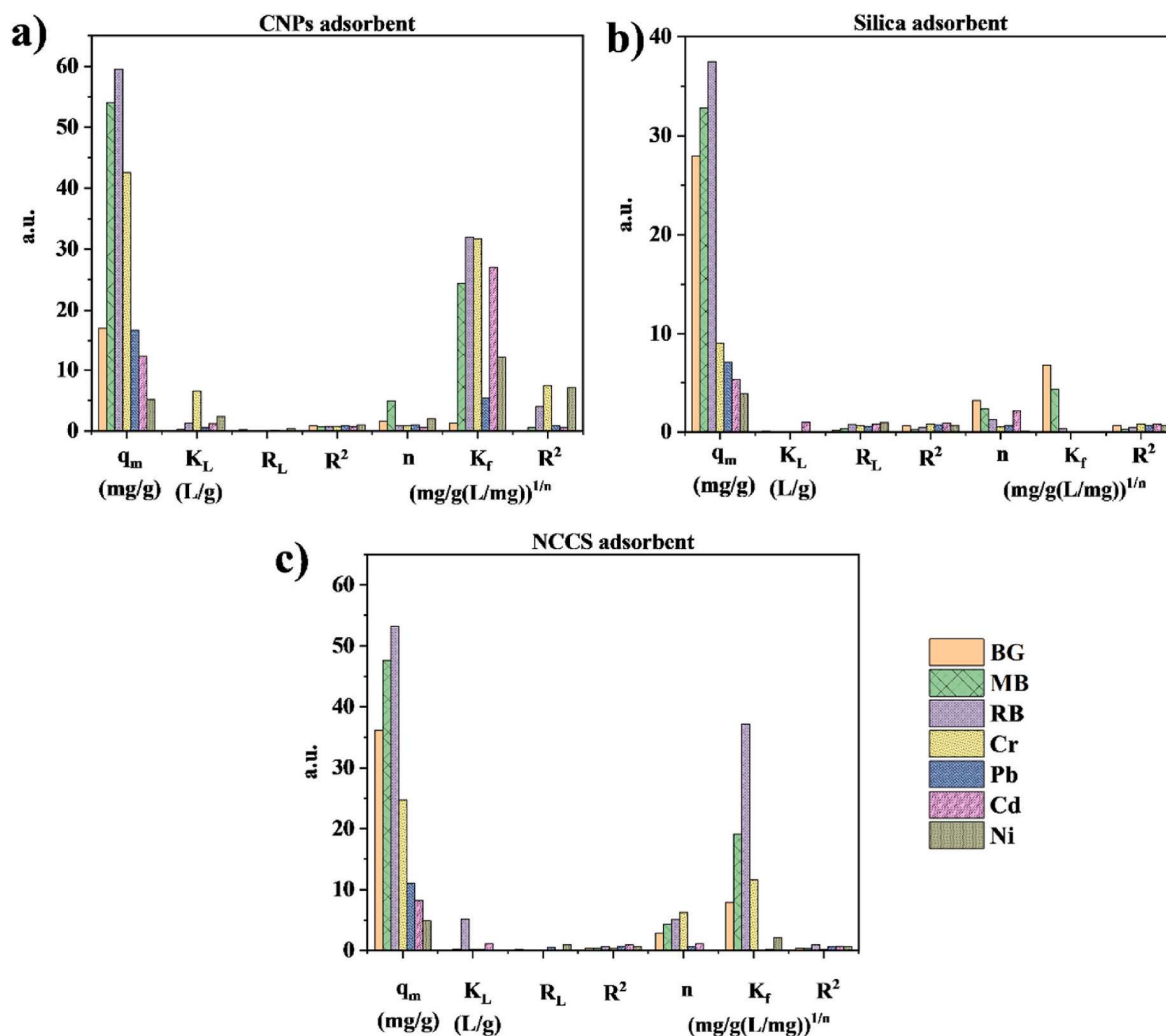


**Fig. 5.** The Langmuir constants ( $q_m$ ,  $K_L$ ,  $R_L$ ,  $R^2$ ) and Freundlich constants ( $n$ ,  $K_f$ ,  $R^2$ ) of (a) CNPs, (b) silica, and (c) NCCS adsorbents for brilliant green (BG), methylene blue (MB), reactive brown (RB), Cr, Pb, Cd and Ni. (For interpretation of the references to colour in this figure legend, the reader is referred to the Web version of this article.)

was observed for RB (59.52 mg/g) among dyes and for  $\text{Cr}^{6+}$  (42.55 mg/g) among HMs. The order of adsorption capacity decreased as  $\text{RB} > \text{Cr}^{6+} > \text{MB} > \text{BG} > \text{Pb}^{2+} > \text{Cd}^{2+} > \text{Ni}^{2+}$ . CNP was found to be most effective in removing HMs, while NCCS showed similar adsorption capacities for HMs and reactive dyes. NCCS demonstrated the best stability for removing reactive dyes and HMs from water, and is recommended for further research in sustainable water pollution control. The adsorption mechanism involved both physisorption and chemisorption from adsorption isotherm and kinetics modelling. In future research, appropriate post-treatment of adsorbents after their application in contaminant removal should be explored for enhancing reuse potential.

#### Ethical approval

Not applicable.

#### Funding

The authors declare that no funds, grants, or other support were received during the preparation of this manuscript.

#### Consent to participate

Not applicable.

#### Consent to publish

All authors support this manuscript for publication.

#### CRediT authorship contribution statement

**Md. Ibrahim H. Mondal:** Writing – review & editing, Supervision, Project administration, Funding acquisition. **Shovra Chandra Chakraborty:** Investigation, Formal analysis. **Md Saifur Rahman:** Writing – original draft. **Shaik Merkatur Hakim Marjuban:** Writing – original draft. **Firoz Ahmed:** Methodology, Formal analysis. **John L. Zhou:** Writing – review & editing, Project administration. **Mohammad Boshir Ahmed:** Writing – review & editing, Project administration. **Masoumeh Zargar:** Writing – review & editing, Formal analysis.

#### Declaration of competing interest

The authors declare that they have no known competing financial interests or personal relationships that could have appeared to influence the work reported in this paper.

#### Data availability

Data will be made available on request.

## Appendix A. Supplementary data

Supplementary data to this article can be found online at <https://doi.org/10.1016/j.envpol.2024.123637>.

## References

- Adam, F., Appaturi, J.N., Iqbal, A., 2012. The utilization of rice husk silica as a catalyst: review and recent progress. *Catal. Today* 190, 2–14.
- Alvarez, J., Lopez, G., Amutio, M., Bilbao, J., Olazar, M., 2014. Bio-oil production from rice husk fast pyrolysis in a conical spouted bed reactor. *Fuel* 128, 162–169.
- Ang, T.N., Ngoh, G.C., Chua, A.S.M., 2013. Comparative study of various pretreatment reagents on rice husk and structural changes assessment of the optimized pretreated rice husk. *Bioresour. Technol.* 135, 116–119.
- Athinarayanan, J., Periasamy, V.S., Alhazmi, M., Alatiyah, K.A., Alshatwi, A.A., 2015. Synthesis of biogenic silica nanoparticles from rice husks for biomedical applications. *Ceram. Int.* 41, 275–281.
- Bădescu, I.S., Bulgariu, D., Ahmad, I., Bulgariu, L., 2018. Valorisation possibilities of exhausted biosorbents loaded with metal ions—a review. *J. Environ. Manag.* 224, 288–297.
- Bakar, M.S.A., Titiloye, J.O., 2013. Catalytic pyrolysis of rice husk for bio-oil production. *J. Anal. Appl. Pyrol.* 103, 362–368.
- Borsagli, F.G.L.M., Borsagli, A., 2019. Chemically modified chitosan bio-sorbents for the competitive complexation of heavy metals ions: a potential model for the treatment of wastewaters and industrial spills. *J. Polym. Environ.* 27, 1542–1556.
- Carmona, V., Oliveira, R., Silva, W., Mattoso, L., Marconcini, J., 2013. Nanosilica from rice husk: extraction and characterization. *Ind. Crops Prod.* 43, 291–296.
- Da'na, E., 2017. Adsorption of heavy metals on functionalized-mesoporous silica: a review. *Microporous Mesoporous Mater.* 247, 145–157.
- Das, S.K., Khan, M.M.R., Parandhaman, T., Laffir, F., Guha, A.K., Sekaran, G., Mandal, A. B., 2013. Nano-silica fabricated with silver nanoparticles: antifouling adsorbent for efficient dye removal, effective water disinfection and biofouling control. *Nanoscale* 5, 5549–5560.
- Duffus, J.H., 2003. Toxicology of metals—science confused by poor use of terminology. *Arch. Environ. Health* 58, 263–266.
- Dyal, A., Loos, K., Noto, M., Chang, S.W., Spagnoli, C., Shafi, K.V., Ulman, A., Cowman, M., Gross, R.A., 2003. Activity of *Candida rugosa* lipase immobilized on  $\gamma$ -Fe<sub>2</sub>O<sub>3</sub> magnetic nanoparticles. *J. Am. Chem. Soc.* 125, 1684–1685.
- Feng, J., Cerniglia, C.E., Chen, H., 2012. Toxicological significance of azy dye metabolism by human intestinal microbiota. *Front. Biosci.* 4, 568.
- Fu, F., Wang, Q., 2011. Removal of heavy metal ions from wastewaters: a review. *J. Environ. Manag.* 92, 407–418.
- Haider, J.B., Haque, M.I., Hoque, M., Hossen, M.M., Mottakin, M., Khaleque, M.A., Johir, M.A.H., Zhou, J.L., Ahmed, M.B., Zargar, M., 2022. Efficient extraction of silica from openly burned rice husk ash as adsorbent for dye removal. *J. Clean. Prod.* 380, 135121.
- He, C., Ren, L., Zhu, W., Xu, Y., Qian, X., 2015. Removal of mercury from aqueous solution using mesoporous silica nanoparticles modified with polyamide receptor. *J. Colloid Interface Sci.* 458, 229–234.
- Huang, Y., Zheng, H., Hu, X., Wu, Y., Tang, X., He, Q., Peng, S., 2022. Enhanced selective adsorption of lead (II) from complex wastewater by DTPA functionalized chitosan-coated magnetic silica nanoparticles based on anion-synergism. *J. Hazard Mater.* 422, 126856.
- Jain, A., Kumari, S., Agarwal, S., Khan, S., 2021. Water purification via novel nano-adsorbents and their regeneration strategies. *Process Saf. Environ. Protect.* 152, 441–454.
- Khonde, R., Chaurasia, A., 2016. Rice husk gasification in a two-stage fixed-bed gasifier: production of hydrogen rich syngas and kinetics. *Int. J. Hydrogen Energy* 41, 8793–8802.
- Kumproa, K., Singhykaew, S., Nuntiya, A., 2012. Effects of reaction time and hydrochloric acid concentration on acid hydrolysis of rice husk by reflux method. *Adv. Mater. Res.* 550, 592–597.
- Liu, F., Wen, L.-X., Li, Z.-Z., Yu, W., Sun, H.-Y., Chen, J.-F., 2006. Porous hollow silica nanoparticles as controlled delivery system for water-soluble pesticide. *Mater. Res. Bull.* 41, 2268–2275.
- Liu, N., Huo, K., McDowell, M.T., Zhao, J., Cui, Y., 2013. Rice husks as a sustainable source of nanostructured silicon for high performance Li-ion battery anodes. *Sci. Rep.* 3, 1919.
- Lü, T., Zhang, S., Qi, D., Zhang, D., Vance, G.F., Zhao, H., 2017. Synthesis of pH-sensitive and recyclable magnetic nanoparticles for efficient separation of emulsified oil from aqueous environments. *Appl. Surf. Sci.* 396, 1604–1612.
- Mauter, M.S., Elimelech, M., 2008. Environmental applications of carbon-based nanomaterials. *Environ. Sci. Technol.* 42, 5843–5859.
- Mojiri, A., Zhou, J.L., Nazari, M., Rezaei, S., Farraji, H., Vakili, M., 2022. Biochar enhanced the performance of microalgae/bacteria consortium for insecticides removal from synthetic wastewater. *Process Saf. Environ. Protect.* 157, 284–296.
- Mojiri, A., Zhou, J.L., Ratnaweera, H., Ohashi, A., Ozaki, N., Aoi, Y., Vakili, M., Kindaichi, T., 2021. Performance optimization of a chitosan/anammox reactor in nitrogen removal from synthetic wastewater. *J. Environ. Chem. Eng.* 9 (3), 105252.
- Mourya, V., Inamdar, N.N., 2008. Chitosan-modifications and applications: opportunities galore. *React. Funct. Polym.* 68, 1013–1051.
- Musilova, J., Arvay, J., Vollmannova, A., Toth, T., Tomas, J., 2016. Environmental contamination by heavy metals in region with previous mining activity. *Bull. Environ. Contam. Toxicol.* 97, 569–575.
- Narayanasamy, S., Sundaram, V., Sundaram, T., Vo, D.V.N., 2022. Biosorbent activity of plant based biosorbents in removing hexavalent chromium from aqueous solutions—Insights into isotherm and kinetic studies. *Environ. Res.* 210, 112902.
- Nguyen, K.T., Navidpour, A.H., Ahmed, M.B., Mojiri, A., Huang, Y., Zhou, J.L., 2022. Adsorption and desorption behavior of arsenite and arsenate at river sediment-water interface. *J. Environ. Manag.* 317, 115497.
- Olivera, S., Muralidhara, H.B., Venkatesh, K., Guna, V.K., Gopalakrishna, K., Kumar, Y., 2016. Potential applications of cellulose and chitosan nanoparticles/composites in wastewater treatment: a review. *Carbohydr. Polym.* 153, 600–618.
- Oulkhir, A., Lyamlouli, K., Danouche, M., Benhida, R., 2023. Biosorption of a cationic dye using raw and functionalized *Chenopodium quinoa* pericarp biomass after saponin glycosides extraction. *J. Environ. Chem. Eng.* 11, 110419.
- Pode, R., 2016. Potential applications of rice husk ash waste from rice husk biomass power plant. *Renew. Sustain. Energy Rev.* 53, 1468–1485.
- Praveen, S., Jegan, J., Bhagavathi Pushpa, T., Gokulan, R., Bulgariu, L., 2022. Biochar for removal of dyes in contaminated water: an overview. *Biochar* 4, 10.
- Rafatullah, M., Sulaiman, O., Hashim, R., Ahmad, A., 2010. Adsorption of methylene blue on low-cost adsorbents: a review. *J. Hazard Mater.* 177, 70–80.
- Rendón, J., Giraldo, C.H., Monyake, K.C., Alagha, L., Colorado, H.A., 2023. Experimental investigation on composites incorporating rice husk nanoparticles for environmental noise management. *J. Environ. Manag.* 325, 116477.
- Salman, M., Jahan, S., Kanwal, S., Mansoor, F., 2019. Recent advances in the application of silica nanostructures for highly improved water treatment: a review. *Environ. Sci. Pollut. Res.* 26, 21065–21084.
- Shamsollahi, Z., Partovinia, A., 2019. Recent advances on pollutants removal by rice husk as a bio-based adsorbent: a critical review. *J. Environ. Manag.* 246, 314–323.
- Shen, Y., Zhao, P., Shao, Q., 2014. Porous silica and carbon derived materials from rice husk pyrolysis char. *Microporous Mesoporous Mater.* 188, 46–76.
- Varma, A., Deshpande, S., Kennedy, J., 2004. Metal complexation by chitosan and its derivatives: a review. *Carbohydr. Polym.* 55, 77–93.
- Waghmare, C., Ghodmare, S., Ansari, K., Dehghani, M.H., Khan, M.A., Hasan, M.A., Islam, S., Khan, N.A., Zahmatkesh, S., 2023. Experimental investigation of H<sub>3</sub>PO<sub>4</sub> activated papaya peels for methylene blue dye removal from aqueous solution: evaluation on optimization, kinetics, isotherm, thermodynamics, and reusability studies. *J. Environ. Manag.* 345, 118815.
- Wang, X., Schröder, H.C., Wiens, M., Ushijima, H., Müller, W.E., 2012. Bio-silica and bio-polyphosphate: applications in biomedicine (bone formation). *Curr. Opin. Biotechnol.* 23, 570–578.
- Yalcin, N., Sevinc, V., 2001. Studies on silica obtained from rice husk. *Ceram. Int.* 27, 219–224.
- Yang, J., Zhen, L., Ren, F., Campbell, J., Rorrer, G.L., Wang, A.X., 2015. Ultra-sensitive immunoassay biosensors using hybrid plasmonic-biosilica nanostructured materials. *J. Biophot.* 8, 659–667.
- Yang, X., Shen, Z., Zhang, B., Yang, J., Hong, W.-X., Zhuang, Z., Liu, J., 2013. Silica nanoparticles capture atmospheric lead: implications in the treatment of environmental heavy metal pollution. *Chemosphere* 90, 653–656.
- Zhang, S., Liu, C., Yuan, Y., Fan, M., Zhang, D., Wang, D., Xu, Y., 2020. Selective, highly efficient extraction of Cr(III), Pb(II) and Fe(III) from complex water environment with a tea residue derived porous gel adsorbent. *Bioresour. Technol.* 311, 123520.
- Zhou, J.L., Salvador, S.M., Liu, Y.P., Sequeira, M., 2001. Heavy metals in the tissues of common dolphins (*Delphinus delphis*) stranded on the Portuguese coast. *Sci. Total Environ.* 273 (1–3), 61–76.
- Zhou, Y.S., Yang, D.Z., Nie, J., 2007. Preparation and characterization of crosslinked chitosan-based nanofibers. *Chin. Chem. Lett.* 18, 118–120.